PHYSICAL REVIEW B **96**, 220303(R) (2017)

Pronounced low-frequency vibrational thermal transport in C_{60} fullerite realized through pressure-dependent molecular dynamics simulations

Ashutosh Giri[1,*] and Patrick E. Hopkins[1,2,3,†]

[1]*Department of Mechanical and Aerospace Engineering, University of Virginia, Charlottesville, Virginia 22904, USA*

[2]*Department of Materials Science and Engineering, University of Virginia, Charlottesville, Virginia 22904, USA*

[3]*Department of Physics, University of Virginia, Charlottesville, Virginia 22904, USA*

(Received 27 October 2017; published 27 December 2017)

Fullerene condensed-matter solids can possess thermal conductivities below their minimum glassy limit while theorized to be stiffer than diamond when crystallized under pressure. These seemingly disparate extremes in thermal and mechanical properties raise questions into the pressure dependence on the thermal conductivity of C_{60} fullerite crystals, and how the spectral contributions to vibrational thermal conductivity changes under applied pressure. To answer these questions, we investigate the effect of strain on the thermal conductivity of C_{60} fullerite crystals via pressure-dependent molecular dynamics simulations under the Green-Kubo formalism. We show that the thermal conductivity increases rapidly with compressive strain, which demonstrates a power-law relationship similar to their stress-strain relationship for the C_{60} crystals. Calculations of the density of states for the crystals under compressive strains reveal that the librational modes characteristic in the unstrained case are diminished due to densification of the molecular crystal. Over a large compression range (0–20 GPa), the Leibfried-Schlömann equation is shown to adequately describe the pressure dependence of thermal conductivity, suggesting that low-frequency intermolecular vibrations dictate heat flow in the C_{60} crystals. A spectral decomposition of the thermal conductivity supports this hypothesis.

DOI: 10.1103/PhysRevB.96.220303

The capability of fabricating bulk C_{60} (fullerite) in large quantities [1,2] has prompted a plethora of research on their physical properties driven by the interest in applications such as photovoltaics [3,4], thermoelectrics [5,6], and phase change memory devices [7]. The clear understanding of thermal transport across these material systems is quintessential for their proper utilization in these applications; for example, Joule heating needs to be accurately accounted for in photovoltaic and phase change memory devices. Likewise, a clear understanding of the intrinsic vibrational thermal transport mechanisms in fullerite crystals is indispensable for their use in thermoelectric devices where materials with glasslike thermal conductivity and metal-like electronic conductivity are generally desired [6,8].

Since its conception, several studies have focused on experimental and theoretical development of the equation of state of C_{60} crystals under compressive stress [9–13]. It has been theorized that the bulk modulus of C_{60} crystals can even exceed that of diamond, the least compressible substance that is presently known [11,12]. However, relatively fewer studies have focused on understanding their thermal properties [14–16], and pressure effects on the thermal conductivity of these novel material systems has been largely unexplored. In this regard, C_{60} films and compacts have been shown to demonstrate thermal conductivities below their respective amorphous/minimum limits under ambient conditions and, in general, low thermal conductivity materials are often not associated with large stiffness/strong bonds.

At room temperature and atmospheric pressure, fullerites are composed of sp^2 bonded C_{60} molecules and the molecular cages are arranged in an fcc lattice with weaker van der Waals bonding between the hollow molecular cages [13]. Therefore, their vibrational density of states (DOS) are occupied by modes that arise due to intermolecular (inter-C_{60}) vibrations, which include the librational and rotational motion of the cages, and those that are the result of intramolecular (intra-C_{60}) vibrations [17]. In terms of their vibrational characteristics, molecular dynamics (MD) simulations have revealed that at temperatures greater than 200 K, C_{60} molecules rotate unhindered at high frequencies, whereas, at lower temperatures, orientational freezing is observed [18,19]. We have previously shown that the dominant contribution to thermal conductivity in the fcc phase of fulllerite originates from the intermolecular modes ($>$2 THz) [20].

For dielectric crystals in general, in which thermal transport is largely phonon mediated, the Leibfried-Schlömann (LS) equation [21–23] is a commonly implemented model to describe the pressure dependence of thermal conductivity. This model is based on the assumption that acoustic phonons carry a significant amount of heat and three phonon scattering processes between the acoustic modes dictate the thermal conductivity. So far, the validity of this model has been tested experimentally for compressed H_2O (and it has been shown to successfully describe the increase in thermal conductivity of H_2O between 2 and 22 GPa) [24]. The model has also successfully been tested for MgO up to pressures of 60 GPa [25] and for muscovite crystals in the cross plane direction (which suggested that acoustic phonons dominate heat transfer in these structures) [26]. However, the applicability of the model for large unit cell crystals (with optical phonons making up a large percentage of the available vibrational modes) has been debated due to the fact that acoustic-optical mode scattering could play a significant role in dictating the thermal conductivity [27,28]. Furthermore, the LS model has been shown to grossly overpredict the thermal conductivity of polymers at high pressures since acoustic phonons with

*ag4ar@virginia.edu

†phopkins@virginia.edu

high group velocities are not the dominant heat carriers in amorphous polymers [29].

In this work, we study the effect of hydrostatic compressions of up to 20 GPa on the thermal properties of C_{60} crystals in the fcc phase via molecular dynamics simulations. We show that the stress-strain relationship along with the strain dependence on thermal conductivity for the C_{60} crystals does not follow a symmetric trend about zero strain; the application of compressive strain leads to the rapid increase in both the thermal conductivity and stress, which demonstrate a power-law dependence on the applied strain. The compressive strain is shown to densify the C_{60} crystal leading to the diminishing characteristics of the librational modes. Along with the rotational modes being hindered due to the applied compressive strains, the shift in the DOS of intermolecular vibrations to higher frequencies is shown to significantly enhance the thermal conductivity. Moreover, the LS equation adequately describes the increase in thermal conductivity of C_{60} crystals suggesting that low-frequency intermolecular modes carry the significant amount of heat in these structures. A spectral decomposition of thermal conductivity supports the hypothesis that low-frequency intermolecular modes dictate the thermal conductivity in C_{60} crystals even at hydrostatic compressive strains of ∼20 GPa.

In accordance with previous computational works focusing on thermal transport across C_{60} crystals [16,20], we utilize the polymer consistent force field (PCFF) to describe the inter- and intramolecular interactions. As pointed out earlier, van der Waals forces dictate the intermolecular interaction, which is modeled by the Lennard-Jones potential included in the PCFF potential. Along with the van der Waals interactions, the bond angles, dihedrals, and improper interactions are also defined in the PCFF potential [30,31]. For our simulations on C_{60} crystals, initially the fullerene molecules are placed in a fcc lattice with a center to center distance of 9 Å and a NPT integration, which is the isothermal-isobaric ensemble with number of particles, pressure, and temperature of the system held constant, is implemented for 1 ns to relax the structure to 0 bar pressure. The equilibrated density of the fullerite with a computational domain size of $55 \times 55 \times 55$ Å^3 and periodic boundary conditions in all three principal directions is 1.75 g cm^{-3}; the experimentally determined density of C_{60} is ∼1.68 g cm^{-3} [32]. A schematic (with the front view) of the equilibrated C_{60} crystal is shown in Fig. 1. After equilibration, hydrostatic pressures of up to 20 GPa are applied and the systems are further equilibrated under the NVT ensemble. The thermal conductivities of the strained crystals under hydrostatic pressure are determined via the Green-Kubo (GK) approach in the microcanonical ensemble; the details of the GK procedure are given in our earlier work [20].

Figure 1(b) shows the MD-predicted thermal conductivities as a function of strain for the C_{60} crystals. The thermal conductivities for the C_{60} crystals demonstrate a rapid increase in thermal conductivity due to compressive strain and a slight decrease in thermal conductivity with tensile strains. It is also interesting to note that the thermal conductivity demonstrates a power law with strain [shown by the solid line in Fig. 1(b)] with rapid increase in thermal conductivity at large hydrostatic compressions. Similar to the thermal conductivity dependence on strain, the stress-strain relationship shown in Fig. 1(c) also depicts a similar trend of rapid increase with compressive strains. This can be related to the densification (or shortening of the distances between the C_{60} molecules in the fcc phase); the density of the C_{60} crystal increases by ∼33% with the application of 9% hydrostatic compressive strain. As a result of the large compressive strain and the concomitant increase in the density, the dynamic motion of the C_{60} molecules is constrained. This is visualized in the inset of Figs. 1(b) and 1(c) where we show the displacement magnitude of the individual atoms after 50 ps with respect to a reference equilibrated state of the computational domain [see scale in the inset of Fig. 1(b)]. As is evident, the C_{60} molecules in the compressed state show a reduced displacement in comparison to the unstrained case, which is due to the hydrostatic strain limiting the librational motion of the individual C_{60} molecules in the fcc phase.

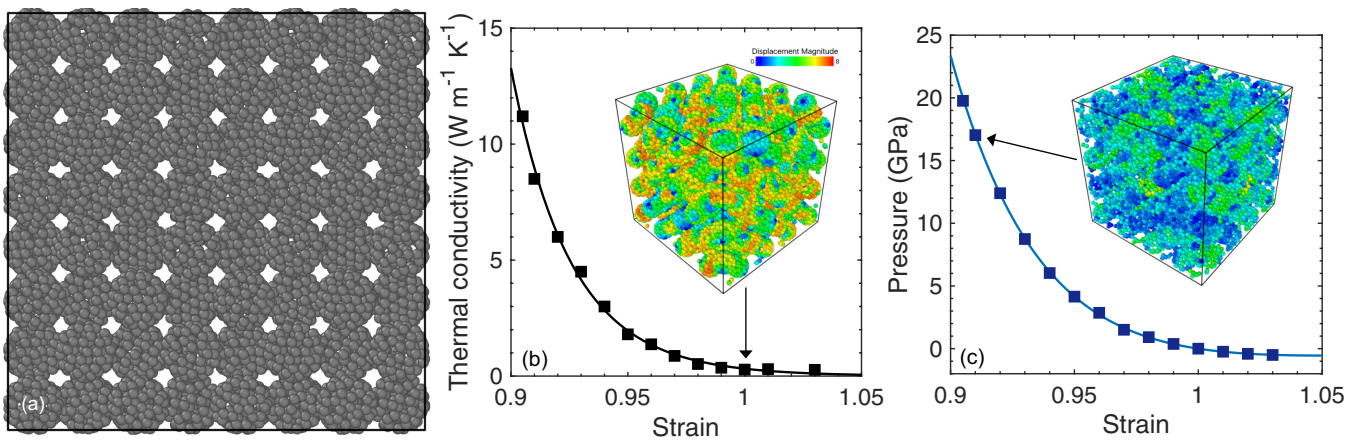

FIG. 1. (a) Schematic of the $55 \times 55 \times 55$ Å^3 periodic computational domain used for Green-Kubo calculations for C_{60} crystals. (b) Thermal conductivity as a function of strain. Inset: Representation of the computational domain for the unstrained case where the colors for the atoms are assigned for displacement magnitude after 50 ps with respect to a reference equilibrated state of the computational domain (see color bar). (c) Stress-strain relationship for C_{60} crystals, which demonstrates a power-law increase similar to the thermal conductivity increase with hydrostatic compressive stress. Inset: Atoms colored according to the displacement magnitude at 9% compressive strain.

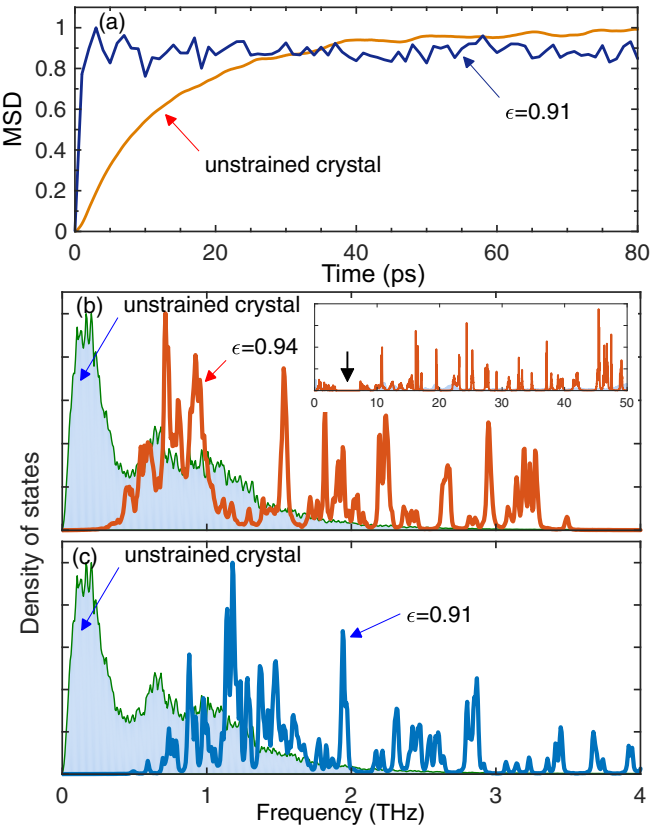

FIG. 2. (a) Normalized MSD of the atoms as a function of time for the C_{60} crystals under unstrained and 9% compressive strain conditions. Vibrational density of states in the low-frequency regime (b) at 6% and (c) 9% compressive strains. The density of states for the librational modes (<0.5 THz) diminishes as the hydrostatic compressive strain is increased.

To quantitatively show that the librational modes are constrained due to the hydrostatic compressive strain, we calculate the mean-square displacement (MSD) of the atoms in the C_{60} crystals as a function of time, which describes their random motion [33]. Figure 2(a) shows the normalized MSD as a function of time for unstrained and 9% hydrostatic compressive strain cases. The slow rise and an order of magnitude higher MSD for the unstrained case has been related to the rotational motion of the C_{60} molecules, and the time constant of the slow rise relates to vibrational modes at ∼0.1 THz [20,33]. The rapid increase in MSD for the strained case suggests that these librational modes are absent due to the densification of the fcc phase. We note that as we are only interested in the effect of strain on the thermal and vibrational properties of the fcc phase of C_{60} crystals, we only consider strain levels of up to 9.5% corresponding to <20 GPa stress. Upon application of further compressive strains >20 GPa, a phase change and polymerization of C_{60} molecules have been observed [9,34].

To gauge the relative effect of compressive strains on the vibrational properties of C_{60} crystal, we calculate the DOS of low-frequency vibrations (corresponding to intermolecular vibrations) for C_{60} crystals under compressive strains of 6% and 9%, respectively [as shown in Figs. 2(b) and 2(c)]. The DOS of the unstrained case is also shown for comparison in the background. Along with the low-frequency DOS, for comparison, we have also included the full DOS for the 6% strained crystal in the inset of Fig. 2(b). The most obvious observation due to the application of hydrostatic compressive strain is the gradual reduction in the DOS of frequencies below ∼0.5 THz. As discussed in the earlier paragraph, these modes are related to the librational modes of the C_{60} molecules. In the unstrained case, a band gap in the vibrational DOS arises in the 2–7 THz range, which marks the transition from inter- to intramolecular vibrations as suggested in Ref. [16]; we have highlighted the band gap with an arrow in the inset of Fig. 2(b) for the case of the 6% strained C_{60} crystal. The modes below ∼2 THz (for the unstrained case) have been prescribed to intermolecular vibrations [16], and in our previous work in Ref. [20], we have shown that these modes that are characteristic of intermolecular vibrations (<2 THz), carry the majority of the heat in the unstrained C_{60} crystal. The application of compressive strain causes stiffening of the intermolecular modes, which leads to the shift in the DOS of the intermolecular vibrational spectrum to higher frequencies as shown in Figs. 2(b) and 2(c). Note, as is expected, the compressive strain leading to densification only causes the intermolecular vibrational spectrum to prominently shift to higher frequencies, whereas the intramolecular vibrations remain largely unaffected due to the application of <20 GPa of hydrostatic compressive stress [these intramolecular vibrations range in the 10–50 THz regime as shown in the inset of Fig. 2(b)]. The resulting increase in the thermal conductivity with increasing compressive strain as shown in Fig. 1(b), therefore, can be largely attributed to the stiffening of intermolecular vibrations and the diminishing characteristics of the librational modes, which in the unstrained case, diffusively scatters with the heat-carrying vibrations, thus resulting in the relatively lower thermal conductivity [20].

In general, for inorganic crystals, the application of a compressive (tensile) strain, the lattice stiffens (softens) and the vibrational frequencies are shifted to a higher (lower) frequency spectrum [35]. Therefore, compressive strain causes a stiffening of modes as evidenced by a depletion in low-frequency vibrations and an enhancement in high-frequency vibrations in comparison to the unstrained system. Conversely, the application of tensile strain will soften the modes that lead to a depletion in the high-frequency vibrational spectrum with a corresponding enhancement in low-frequency modes. It has been shown that increase in stiffness leads to higher phonon group velocities and the concomitant increase in thermal conductivity [36,37]. In addition, molecular dynamics simulations of Lennard-Jones argon have shown that phonon lifetimes decrease as the system is exposed to strain levels from compression to tension [36]. This suggests that the increase in thermal conductivity for our C_{60} crystals with the application of compressive stress can largely be attributed to both the higher phonon group velocities and larger phonon lifetimes that derive from the stiffening of the intermolecular vibrational modes.

In terms of an analytical description of strain-dependent thermal conductivity, Leibfried and Schlömann [21] showed that for an isotropic solid, under isochoric conditions with monatomic basis, the thermal conductivity can be estimated

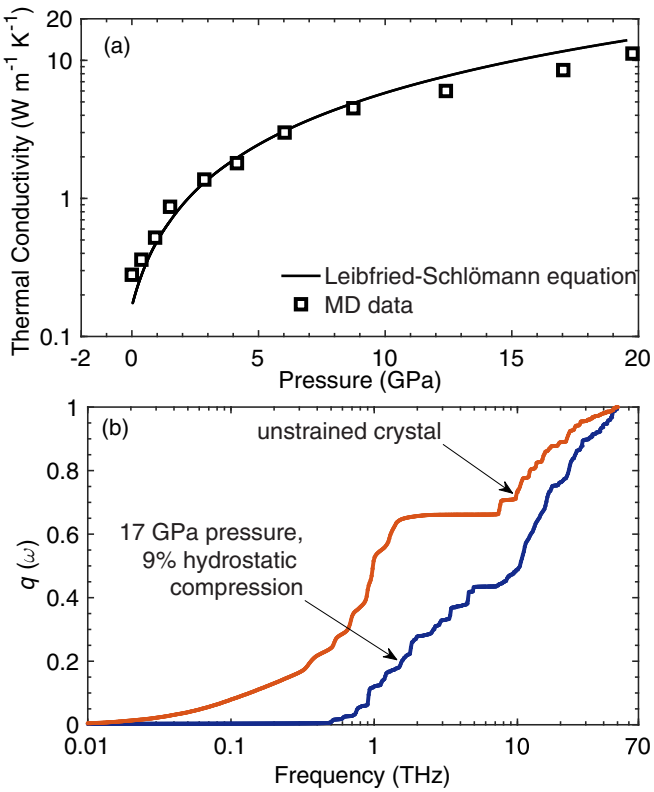

FIG. 3. (a) MD-predicted thermal conductivity of C_{60} crystal up to 20 GPa compressive stress at 300 K. The results from the Leibfried-Schlömann equation are also plotted for comparison. (b) Spectral contributions to thermal conductivity for unstrained and strained (under 9% hydrostatic strain) cases.

as [22,38]

$$\kappa = A\frac{V^{1/3}\omega_D^3}{\gamma^2 T}, \tag{1}$$

where A is a parameter independent of pressure, V is the volume, ω_D is the Debye frequency, γ is the Grüneisen parameter, and T is the temperature. In this expression, anharmonicity is included through the Grüneisen parameter, $\gamma = -(\partial \ln\omega)/(\partial \ln V)$, where ω is the frequency of lattice vibration and V represents the volume [39]. If we assume that the Poisson's ratio and elastic anisotropy does not change with the application of compressive strains, then $\omega_D \propto V^{1/6}K_T^{1/2}$, where K_T is the isothermal bulk modulus which can be calculated as $K_T = -dP/d\ln V$. For our C_{60} crystals, we calculate $K_T \sim 10$ and 250 GPa for the unstrained and the strained crystal at 9.5% hydrostatic strain, respectively. The Gruneisen parameter γ is determined from the relation $\gamma = \frac{1}{2}\frac{dK}{dP} - \frac{1}{6}$. Figure 3(a) shows the results of the LS theory as a function of pressure. The model adequately describes the MD simulation results over the large range of pressures considered in this work confirming its usefulness as a model to describe the pressure dependence of thermal conductivity of molecular crystals with more than one atom forming the unit cell. The agreement between theory and MD simulation results also suggests that the dominant heat carriers in the C_{60} crystal are the acoustic phonons which arise due to intermolecular vibrations.

To study the spectral nature of thermal conductivity with the application of compressive strains for our C_{60} crystal, we spectrally resolve the thermal conductivity by calculating the contribution of each mode to the heat flux; the details of the calculation are given in our previous work [40]. Figure 3(b) shows the normalized thermal conductivity accumulation for the unstrained and 9% hydrostatic compression cases. For the unstrained case, as we report in our previous work, the majority of the heat is carried by modes that are <2 THz. These modes shift to higher frequencies with the compressive strain as mentioned in the previous paragraph, and therefore the thermal conductivity accumulation shifts to higher frequencies for the strained case. However, even for the 9% hydrostatic compression case, a significant amount of heat is carried by intermolecular vibrations (<10 THz contribute more than 50% to the thermal conductivity) thus confirming the results from the LS theory that low-frequency vibrations dictate thermal conductivity for the C_{60} crystals under compressive strains.

We have studied the effect of pressure (up to 20 GPa) on the thermal and vibrational properties of C_{60} fullerite crystals via molecular dynamics simulations under the GK formalism. The pressure dependence of thermal conductivity of C_{60} fullerite was found to obey a power-law dependence on the applied strain with compressive strains leading to a rapid increase in the thermal conductivity. At a hydrostatic pressure of ~20 GPa the thermal conductivity of C_{60} fullerite increases by almost a factor of 40 (compared to the thermal conductivity at ambient conditions). The Leibfried-Schlömann equation adequately describes the pressure dependence of thermal conductivity in these materials suggesting that low-frequency acoustic modes carry the significant amount of heat in these crystals. This theoretical description is supported by spectral analysis of heat current in C_{60} crystals, which shows that the majority of heat is carried by low-frequency intermolecular vibrations.

We would like to thank the Army Research Office for support (Grant No. W911NF-16-1-0320).

[1] H. Kroto, Science **242**, 1139 (1988).
[2] W. Kratschmer, L. D. Lamb, K. Fostiropoulos, and D. R. Huffman, Nature (London) **347**, 354 (1990).
[3] P. Blom, V. Mihailetchi, L. Koster, and D. Markov, Adv. Mater. **19**, 1551 (2007).
[4] R. Saran, V. Stolojan, and R. J. Curry, Sci. Rep. **4**, 5041 (2014).
[5] M. Sumino, K. Harada, M. Ikeda, S. Tanaka, K. Miyazaki, and C. Adachi, Appl. Phys. Lett. **99**, 093308 (2011).
[6] K. Zhang, Y. Zhang, and S. Wang, Sci. Rep. **3**, 3448 (2013).
[7] C. Kim, D.-S. Suh, K. H. P. Kim, Y.-S. Kang, T.-Y. Lee, Y. Khang, and D. G. Cahill, Appl. Phys. Lett. **92**, 013109 (2008).
[8] M. Dresselhaus, G. Chen, M. Tang, R. Yang, H. Lee, D. Wang, Z. Ren, J.-P. Fleurial, and P. Gogna, Adv. Mater. **19**, 1043 (2007).

[9] S. J. Duclos, K. Brister, R. C. Haddon, A. R. Kortan, and F. A. Thiel, Nature (London) **351**, 380 (1991).
[10] Y. Wang, D. Tománek, and G. F. Bertsch, Phys. Rev. B **44**, 6562 (1991).
[11] R. S. Ruoff and A. L. Ruoff, Appl. Phys. Lett. **59**, 1553 (1991).
[12] R. S. Ruoff and A. L. Ruoff, Nature (London) **350**, 663 (1991).
[13] L. A. Girifalco, Phys. Rev. B **52**, 9910 (1995).
[14] R. C. Yu, N. Tea, M. B. Salamon, D. Lorents, and R. Malhotra, Phys. Rev. Lett. **68**, 2050 (1992).
[15] J. R. Olson, K. A. Topp, and R. O. Pohl, Science **259**, 1145 (1993).
[16] L. Chen, X. Wang, and S. Kumar, Sci. Rep. **5**, 12763 (2015).
[17] J. Yu, R. K. Kalia, and P. Vashishta, Appl. Phys. Lett. **63**, 3152 (1993).
[18] A. Cheng and M. L. Klein, J. Phys. Chem. **95**, 6750 (1991).
[19] A. Cheng and M. L. Klein, Phys. Rev. B **45**, 1889 (1992).
[20] A. Giri and P. E. Hopkins, J. Phys. Chem. Lett. **8**, 2153 (2017).
[21] G. Leibfried and E. Schlömann, Nach. Akad. Wiss. Gottingen, Math. Phyz. Klasse **4**, 71 (1954).
[22] M. Roufosse and P. G. Klemens, Phys. Rev. B **7**, 5379 (1973).
[23] G. A. Slack and R. G. Ross, J. Phys. C **18**, 3957 (1985).
[24] B. Chen, W.-P. Hsieh, D. G. Cahill, D. R. Trinkle, and J. Li, Phys. Rev. B **83**, 132301 (2011).
[25] D. A. Dalton, W.-P. Hsieh, G. T. Hohensee, D. G. Cahill, and A. F. Goncharov, Sci. Rep. **3**, 2400 (2013).
[26] W.-P. Hsieh, B. Chen, J. Li, P. Keblinski, and D. G. Cahill, Phys. Rev. B **80**, 180302 (2009).
[27] E. F. Steigmeier and I. Kudman, Phys. Rev. **141**, 767 (1966).
[28] A. Ward, D. A. Broido, D. A. Stewart, and G. Deinzer, Phys. Rev. B **80**, 125203 (2009).
[29] W.-P. Hsieh, M. D. Losego, P. V. Braun, S. Shenogin, P. Keblinski, and D. G. Cahill, Phys. Rev. B **83**, 174205 (2011).
[30] J. R. Maple, U. Dinur, and A. T. Hagler, Proc. Natl. Acad. Sci. USA **85**, 5350 (1988).
[31] H. Sun, Macromolecules **28**, 701 (1995).
[32] J.-H. Pohls, M. B. Johnson, and M. A. White, Phys. Chem. Chem. Phys. **18**, 1185 (2016).
[33] X. Chen, A. Weathers, J. Carrete, S. Mukhopadhyay, O. Delaire, D. A. Stewart, N. Mingo, S. N. Girard, J. Ma, D. L. Abernathy, J. Yan, R. Sheshka, D. P. Sellan, F. Meng, S. Jin, J. Zhou, and L. Shi, Nat. Commun. **6**, 6723 (2015).
[34] M. Alvarez and J. Hodeau, Carbon **82**, 381 (2015).
[35] S. Bhowmick and V. B. Shenoy, J. Chem. Phys. **125**, 164513 (2006).
[36] K. D. Parrish, A. Jain, J. M. Larkin, W. A. Saidi, and A. J. H. McGaughey, Phys. Rev. B **90**, 235201 (2014).
[37] R. C. Picu, T. Borca-Tasciuc, and M. C. Pavel, J. Appl. Phys. **93**, 3535 (2003).
[38] R. G. Ross, P. Andersson, B. Sundqvist, and G. Backstrom, Rep. Prog. Phys. **47**, 1347 (1984).
[39] J. C. Slater, *Introduction To Chemical Physics*, 1st ed. (McGraw-Hill, New York, 1939).
[40] A. Giri, J. L. Braun, and P. E. Hopkins, J. Phys. Chem. C **120**, 24847 (2016).